LBNL-39717
UC-414
Preprint

ERNEST ORLANDO LAWRENCE
BERKELEY NATIONAL LABORATORY

Varying Chromaticity: A Damping Mechanism for the Transverse Head-Tail Instability

Wen-Hao Cheng, Andrew M. Sessler,
and Jonathan S. Wurtele
Accelerator and Fusion Research Division

December 1996
Submitted to
Physical Review E

LOAN COPY
Circulates
For 4 weeks

Bldg. 50 Library
Lawrence Berkeley National Laboratory

Copy 2

LBNL-39717

LBNL-39717
CBP Note-199
UC-414

Varying Chromaticity: A Damping Mechanism for the Transverse Head-Tail Instability *

Wen-Hao Cheng[1],
Andrew M. Sessler[2], and Jonathan S. Wurtele[1,2]
[1]Department of Physics, University of California
Berkeley, California 94720 USA
[2]Ernest Orlando Lawrence Berkeley National Laboratory
Berkeley, CA 94720 USA

December 1996

* This work was supported by the Director, Office of Energy Research, Office of High Energy and Nuclear Physics, Division of High Energy Physics, of the U.S. Department of Energy under Contracts No. DE-AC 03-76SF00098 and DE-FG 03-95ER40936.

Varying Chromaticity: A Damping Mechanism for the Transverse Head-Tail Instability *

Wen-Hao Cheng[1], Andrew M. Sessler[2], and Jonathan S. Wurtele[1,2]
[1]Department of Physics, University of California, Berkeley
Berkeley, California 94720
[2]Lawrence Berkeley National Laboratory
Berkeley, California 94720
(Received)

A detailed analytical and numerical study of the suppression of the transverse head-tail instability by modulating the chromaticity over a synchrotron period is presented. We find that a threshold can be developed, and it can be increased to a value larger than the strong head-tail instability threshold. The stability criterion derived agrees very well with the simulations. The underlying physical mechanisms of the damping scheme are the rotation of the head-tail phase such that the instability does not occur, and the Landau damping due to the incoherent betatron tune spread generated by the varying chromaticity.

I. INTRODUCTION

A bunched beam traveling in a vacuum chamber creates a deflecting force generated by the interaction of particles and environment. The deflecting force, the so-called wake field, reacts and perturbs the beam, often causing transverse collective instabilities. These instabilities limit the peak current in the bunch. In this paper, we analyze a new method for controlling such instabilities; namely, through a temporal variation of the ring parameters. We apply this method to a practical example, the head-tail (HT) instability [1].

In a storage ring, particles with different energies see different focusing strengths in quadrupoles, and thus have different betatron frequencies. The ratio of the relative frequency difference to the relative momentum difference is called the chromaticity. The betatron frequency of an off-momentum particle is given by

$$\omega_\beta(\delta) = \omega_{\beta 0}(1 + \xi\delta), \tag{1}$$

where ξ is the chromaticity, $\omega_{\beta 0}$ is the betatron angular frequency of the on-momentum particle, and $\delta = \Delta p/p$ is the relative momentum difference. Even if $\xi = 0$, there is an instability in the particle's transverse motion called the strong head-tail (SHT) instability. This instability has a threshold created by the synchrotron oscillation, and when the threshold is exceeded, the bunch's transverse motion grows exponentially. In practice, $\xi \neq 0$, there is still a SHT instability in transverse motion with a threshold; in addition, there is the head-tail instability due to chromatic effect, which has no stability threshold. The HT instability was observed in experiments [2], has been well analyzed [3], and has been confirmed by simulations [4]. The HT instability has been a concern for many circular accelerators. For example, we may note the observations and simulations of single-bunch transverse excitation of the beam in the proton ring of the HERA collider at DESY [5], the observation of higher-order HT instability in the PS Booster of the LHC at CERN [6], and the investigation of the possible HT oscillation due to a transverse feedback kicker at KEK's B-Factory (KEKB) [7].

It is understood that, when $\xi/\eta > 0$, the bunch's transverse center of motion which is governed by the in-phase mode of head-tail oscillation is damped, while the bunch's transverse size which is governed by the out-of-phase mode of head-tail oscillation grows exponentially; when $\xi/\eta < 0$, the condition reverses [8], where $\eta = pdC/Cdp - 1/\gamma^2$ is the slippage factor, $C = 2\pi R = cT_0$ is the circumference of the ring, $\gamma = (1-\beta^2)^{-1/2}$, and $\beta = v/c \lesssim 1$ for a relativistic beam discussed in this paper. Moreover, the growth rate of the out-of-phase mode when $\xi/\eta > 0$, is smaller than the growth rate of the in-phase mode when $\xi/\eta < 0$. Consequently, machine parameters are usually chosen such that ξ/η is positive and small, i.e. we need $\xi > 0 (< 0)$ when the machine is operated above (below) transition. Damping mechanisms, such as radiation damping and Landau damping, may or may not stabilize the HT instability, depending on the damping time, the width of the incoherent tune spread, and so on.

As the sign of ξ/η is crucial to the stability of the two fundamental modes of head-tail oscillation, in analogy to the strong focusing principle, alternating the sign of ξ/η within a synchrotron period could stabilize both modes. Since

*Work supported by the U.S. Department of Energy under contracts No. DE-FG-03-95ER40936 and DE-AC-03-76SF00098.

varying η means transition crossing, which involves many undesirable problems, such as vanishing Landau damping, large momentum spread, bunch-shape mismatch and nonlinear effects [9]; we propose, in this paper, variation of the chromaticity in order to stabilize the HT instability.

While drafting this paper, we were advised of the existence of the paper written by T. Nakamura of SPring-8 [10]. Nakamura suggested, as we have also (independently), the concept of chromaticity modulation, which contributes an incoherent tune spread that effectively Landau damps the transverse instabilities. In this paper, going considerably beyond what Nakamura has done, we provide analysis, simulation results, and a stability criterion for the head-tail instability.

The chromaticity is considered a function of "time" s, where s measures the distance around the ring. We restrict our analysis to functions that are periodic with the synchrotron period. The chromaticity can thus be expanded in a Fourier series in terms of the harmonics of the synchrotron phase advance ϕ, as

$$\xi(s) = \sum_{n=0} \xi_n \cos(n\phi + \theta_n), \tag{2}$$

where $\phi = \omega_s s/c$, ω_s is the synchrotron angular frequency, $n = 0$ corresponds to the case of constant chromaticity (DC) ξ_0, and θ_n is the phase difference between the chromaticity and energy variation.

The introduction of a time dependent part of the chromaticity generates an additional incoherent tune spread that contributes to the Landau damping, as was emphasized by Nakamura . Specifically, the constant component of the chromaticity causes the HT instability. As will be shown in this paper, the varying part of the chromaticity does not cause a HT instability, and consequently, Landau damping due to the AC (e.g., n=1) incoherent tune spread suppresses the instability due to the DC part of the chromaticity.

The incoherent chromatic tune spread due to ξ_1 can be estimated as

$$\begin{aligned} \sigma_\nu &= \nu_{\beta 0}\xi_1\sqrt{\langle(\delta\sin\phi)^2\rangle} \\ &= \sqrt{3/8}\, g_\sigma \nu_{\beta 0}\xi_1\sigma_\delta, \end{aligned} \tag{3}$$

where $\nu_{\beta 0} = \omega_{\beta 0}/\omega_0$, $\omega_0 = c/R$, $\sigma_\delta = (\omega_s/c\eta)\sigma_z$, σ_z is the rms bunch length, $g_\sigma = \sqrt{\langle r_z^2\rangle_{r_z}}/\sigma_z$ which is a geometric factor depends on the longitudinal distribution $\psi_{0z}(r_z)$, and $\langle\ \rangle = \langle\ \rangle_{r_z}\langle\ \rangle_\phi$,

$$\langle f(r_z)\rangle_{r_z} = \frac{\int_0^\infty dr_z r_z f(r_z)\psi_{0z}(r_z)}{\int_0^\infty dr_z r_z \psi_{0z}(r_z)}, \tag{4}$$

$$\langle f(\phi)\rangle_\phi = \frac{1}{2\pi}\int_0^{2\pi} d\phi f(\phi). \tag{5}$$

For a Gaussian distribution, $g_\sigma = 1$. In obtaining Eq. (3), we have adjusted θ_1 such that the chromaticity modulation is in-phase with the energy oscillation, i.e. $\xi = \xi_0 + \xi_1\sin\phi$, $\delta = (\omega_s/c\eta)r_z\sin\phi$, where (r_z, ϕ) are the action-angle variables in the longitudinal phase space. Note that, the cross-term of ξ_0 and ξ_1 vanishes because $\langle\sin^3\phi\rangle_\phi = 0$. The AC part of the incoherent tune spread contributes to a Landau damping without driving the HT instability [as will be shown], and the damping rate per turn can be approximated as

$$\tau_{LD}^{-1}[1/\text{turn}] \approx 2\pi\sigma_\nu = 2\pi\sqrt{3/8}\, g_\sigma \nu_s \chi_1, \tag{6}$$

where $\nu_s = \omega_s/\omega_0$, and $\chi_1 = \omega_{\beta 0}\xi_1\sigma_z/c\eta$ is the AC part of head-tail phase. Note that the Landau damping time due to the AC part of chromaticity is independent of the beam intensity and the impedance of a ring. In Figs. 1 and 2, we show that, when there is no HT instability ($\chi_0 = 0$), the formula for the Landau damping rate is confirmed by simulations of a bunched beam traversing an averaged impedance in a storage ring [cf. Appendix A]. The implication is that, within the tolerance of dynamic aperture reduction due to the chromaticity, one can increase the damping rate (by a large enough χ_1) to suppress the HT instability.

In Sec. II, a Vlasov analysis is presented. We examine the growth rates for beams with a hollow distribution and with a Gaussian distribution, where both the contributions of the AC and DC are included. Results of macro-particle simulation are discussed.

In Sec. III, the effect of Landau damping, which is not considered in Sec. II, is included by the method of singular eigenfunction expansion. We provide an approximate stability criterion, and study the dispersion relation which includes the incoherent tune spread. We compare the stability limit with macro-particle simulations.

Conclusion is given in Sec. IV.

II. VLASOV ANALYSIS

In this section, we derive the linear eigenmode equation which includes both the DC and AC parts of the chromaticity. The effect of incoherent tune spread is not included, and will be included in the next section. We also study the coherent tune shift of a hollow beam and a Gaussian beam in the longitudinal phase space, in terms of the three parameters: χ_0, χ_1 and Υ.

For an analysis of the effect of varying chromaticity, we assume the particle in a bunched beam experiences two forces: the external focusing force and the wake force generated from the interaction between the beam and cavities. The transverse equation of motion for a particle in a bunch is

$$y''(z,s) + \frac{\omega_\beta^2(\delta)}{c^2} y(z,s) = -\frac{r_0}{\gamma C}\int_z^\infty dz' \rho(z') W_\perp(z-z') y(z',s), \tag{7}$$

where $y(z)$ is the transverse (longitudinal) oscillation coordinate with respect to the bunch center, $' = d/ds$, $N = \int dz'\rho(z')$ is the number of particles in a bunch, $r_0 = e^2/m_0c^2$, $W_\perp$ is the transverse wake function, and particle's energy is $E = \gamma m_0 c^2$.

In the following study, we neglect the nonlinear oscillation due to the rf bucket of the accelerating cavities, or the α bucket of the quasi-isochronous lattice [11]; we also neglect the longitudinal wake force and the gradient of the transverse wake force, which both affect the longitudinal motion. The synchrobetatron coupling effect on the longitudinal orbit is also ignored.

There are two parameters essential to the dynamics studied in this paper:

$$\chi_n = \omega_{\beta 0}\xi_n \sigma_z/c\eta, \tag{8}$$

$$\Upsilon \equiv \pi N r_0 |W_\perp| c^2/8\gamma C \omega_{\beta 0}\omega_s, \tag{9}$$

where χ_n is the phase shift between the head and the tail of a bunch for each harmonic n of the chromaticity. The parameter Υ is approximately the ratio of betatron tune shift to the synchrotron tune. It can easily be shown, by a two particle model, that the onset of the SHT instability is where $\Upsilon \geq 1$ [8], when $\chi_1 = 0$. The well-known transverse Boussard criterion is also consistent with this condition [12].

We have studied a two-particle model incorporating the varying chromaticity scheme. We find that the two-particle model, in contrast to the Vlasov model and the multi-particle simulations, does not demonstrate the effectiveness of the varying chromaticity in damping the HT instability. Physically speaking, it is because a two-particle system does not adequately exhibit the effect of Landau damping.

In this paper, we concentrate on the case of $n = 0$ & 1, therefore we have three independent parameters under study: χ_0, χ_1 and Υ. A larger periodicity of modulation, i.e. $n > 2$, is of course also possible. However, it can be shown that n must be an odd number, such that the ξ_n does not cause instability [cf. Appendix B].

The nonlinear chromaticity characterized by ξ_{01}, when ξ_{DC} is expanded as $\xi_{DC} = \xi_0 + \xi_{01}\delta$, plays a similar role to the AC component ξ_1. In fact, $\xi_1 \simeq \xi_{01}\sigma_\delta$. Since both ξ_{01} and σ_δ are usually small, the nonlinear part of the DC component ξ_{01} is not effective enough to suppress the HT instability. Unless a machine has a large enough $\xi_{01}\sigma_\delta$, one needs to modulate the sextupole magnets to have the value of ξ_1 large enough, so that the damping effect overcomes the instability.

A. Eigenmode Equation

We now present a Vlasov analysis of a many-particle system. We first write down expressions for the dynamical variables in the four dimensional phase space $(z, y; \delta, y')$, in terms of the action-angle variables, as

$$z = r_z \cos\phi_z, \quad \delta = \frac{\omega_s}{\eta c} r_z \sin\phi_z, \tag{10}$$

$$y = r_y \cos\phi_y, \quad y' = -\frac{\omega_{\beta 0}}{c} r_y \sin\phi_y, \tag{11}$$

where $\phi_{(z,y)} = \omega_{(s,\beta 0)} s/c$. The linearized Vlasov equation can then be expressed as

$$-i\frac{\Omega}{c}\psi_1 + \frac{\omega_{\beta 0}}{c}\frac{\partial \psi_1}{\partial \phi_y} + \frac{\omega_s}{c}\frac{\partial \psi_1}{\partial \phi_z} + \frac{F_y(z,s)}{E}\frac{\partial \psi_0}{\partial y'} \approx 0, \tag{12}$$

where the distribution function is expanded as $\psi = \psi_0 + \psi_1 \exp(-i\Omega s/c)$, and Ω is the mode frequency. Eq. (12) can be solved by [8]: (1) the decomposition of the unperturbed and perturbed distribution functions as

$$\psi_0 = \psi_{0z}(r_z)\psi_{0y}(r_y), \quad \psi_1 = \psi_{1z}(r_z,\phi_z)\psi_{1y}(r_y,\phi_y); \tag{13}$$

(2) assuming

$$\psi_{1y}(r_y,\phi_y) = -\langle y\rangle \psi'_{0y}(r_y)e^{i\phi_y}, \tag{14}$$

which describes the transverse dipole oscillation; and (3) using a linear model of the deflecting force given by

$$F_y(z,s) = i\frac{\langle y\rangle e^2}{CT_0}e^{-i\Omega s/c}\sum_q \tilde{\rho}_1(\omega_q)Z_1^{\perp}(\omega_q)e^{i\omega_q z/c}, \tag{15}$$

where $\omega_q = q\omega_0 + \omega_\beta + l\omega_s$,

$$\rho_1(z) = \int d\delta\ \psi_{1z}(r_z,\phi_z), \tag{16}$$

$\int dz\, d\delta \psi_{0z} = N$, and $Z_1^{\perp}(\omega)$ is the total transverse impedance of the ring. The linearized Vlasov equation, including the chromatic term, therefore becomes

$$\left[i\left(\Omega - \omega_{\beta 0}\right)\psi_{1z} - \omega_s\frac{\partial \psi_{1z}}{\partial \phi_z}\right]e^{i\phi_y} - \frac{c^2 r_0\,\psi_{0z}}{2\gamma\omega_{\beta 0}CT_0}\times$$
$$\left(e^{i\phi_y} - e^{-i\phi_y}\right)\sum_q \tilde{\rho}_1(\omega_q)Z_1^{\perp}(\omega_q)e^{i\omega_q r_z\cos\phi_z/c} = 0. \tag{17}$$

Let the longitudinal perturbed distribution function be Fourier expanded as

$$\psi_{1z} = \sum_l \alpha_l R_l(r_z)e^{i(l\phi_z - \Phi)}, \tag{18}$$

where

$$\Phi = \omega_{\beta 0}\int \frac{ds}{c}\,\xi\delta$$
$$= -\frac{\omega_{\xi 0}}{c}r_z\cos\phi_z - \frac{\omega_{\xi 1}}{4c}r_z\cos(2\phi_z), \tag{19}$$

and $\omega_{\xi(0,1)} = \omega_{\beta 0}\xi_{(0,1)}/\eta$, when $\xi = \xi_0 + \xi_1\cos\phi_z$. In this section, we attempt to find the growth rate of the HT instability, the effect of incoherent tune spread which will be illustrated in Sec. III, is ignored here. We now apply

$$\frac{1}{(2\pi)^2}\int_0^{2\pi} d\phi_z\, e^{-il'\phi_z + i\Phi}\int_0^{2\pi} d\phi_y\, e^{-i\phi_y}, \tag{20}$$

on both sides of Eq. (17), in which ψ_{1z} is replaced by Eq. (18). We then obtain the eigenmode equation

$$\left(\Omega - \omega_{\beta 0} - l\omega_s\right)\alpha_l R_l(r_z)$$
$$= i\frac{4\omega_s\Upsilon}{\pi N W_{\perp}T_0}\psi_{0z}(r_z)\sum_q \tilde{\rho}_1(\omega_q)Z_1^{\perp}(\omega_q)I_l(\omega_q), \tag{21}$$

where, by using the generating functions of Bessel functions

$$e^{\pm ix\cos\phi} = \sum_m i^{\pm m}J_m(x)e^{im\phi}, \tag{22}$$

$$e^{\pm ix\sin\phi} = \sum_m i^{\mp m}J_m(x)e^{im\phi}e^{im\pi/2}, \tag{23}$$

and Eq. (16),

$$
\begin{aligned}
& I_l(\omega_q) \\
& = \left\langle e^{-il\phi_z + i(\omega_q - \omega_{\xi 0})(r_z/c)\cos\phi_z - i\omega_{\xi 1}(r_z/4c)\cos(2\phi_z)} \right\rangle_{\phi_z} \\
& = i^l G_q^{(l)*}\left(\frac{\omega_{\xi 1}}{4c} r_z, \frac{\omega_q - \omega_{\xi 0}}{c} r_z\right),
\end{aligned} \tag{24}
$$

$$
\begin{aligned}
\tilde{\rho}_1(\omega_q) &= \int dz e^{-i\omega_q z/c}\rho_1(z) \\
&= 2\pi\frac{\omega_s}{c\eta}\sum_{l'} i^{-l'}\alpha_{l'}\int_0^\infty dr_z' \times \\
&\quad r_z' R_{l'}(r_z') G_q^{(l')}\left(\frac{\omega_{\xi 1}}{4c} r_z', \frac{\omega_q - \omega_{\xi 0}}{c} r_z'\right),
\end{aligned} \tag{25}
$$

and

$$
\begin{aligned}
& G_q^{(l)}\left(\frac{\omega_{\xi 1}}{4c} r_z, \frac{\omega_q - \omega_{\xi 0}}{c} r_z\right) \\
& = \sum_m i^{-m} J_m\left(\frac{\omega_{\xi 1}}{4c} r_z\right) J_{2m+l}\left(\frac{\omega_q - \omega_{\xi 0}}{c} r_z\right).
\end{aligned} \tag{26}
$$

Note that, when $\xi_1 = 0$, Eq. (21) is the eigenmode equation for the case of constant chromaticity [8], where $G_q^{(l)}(x_q) = J_l(x_q)$.

B. Degenerate Radial Mode

The eigenmode equation shown in Eq. (21) can be simplified by assuming a hollow distribution,

$$
\psi_{0z}(r_z) = \frac{N\eta c}{2\pi\omega_s\hat{z}}\delta(r_z - \hat{z}), \tag{27}
$$

where the radial perturbation occurs only on the surface of a delta shell in longitudinal phase space, i.e. $R_l(r_z) \propto \delta(r_z - \hat{z})$. For the zero order perturbation, $\alpha_{l'}^{(l)} = \delta_{ll'}$, $\Omega^{(l)} = \omega_{\beta 0} + l\omega_s$. The mode frequency of the first order perturbation, for the lth mode, is then [cf. Eqs. (21)-(25)]

$$
\begin{aligned}
& \left(\Omega^{(l)} - \omega_{\beta 0} - l\omega_s\right) \\
& = i\frac{4\omega_s\Upsilon}{\pi W_\perp T_0}\sum_q Z_1^\perp(\omega_q)\left|G_q^{(l)}(\frac{\chi_1}{4}, \chi_q - \chi_0)\right|^2,
\end{aligned} \tag{28}
$$

where $\chi_q = \omega_q\hat{z}/c = (q\omega_0 + \omega_{\beta 0} + l\omega_s)\hat{z}/c$, and $\chi_{(0,1)} = \omega_{\xi(0,1)}\hat{z}/c$.

With Eq. (28), we can now find the growth rate, which is the imaginary part of the mode frequency. For a broad-band impedance, the growth rate of the head-tail instability per synchrotron period, given in terms of the imaginary part of the mode frequency, is then

$$
1/\tau_s^{(l)} = -\frac{4\Upsilon}{\pi}\int d\omega_q \tilde{Z}_r(\omega_q)\left|G_q^{(l)}(\frac{\chi_1}{4}, \chi_q - \chi_0)\right|^2, \tag{29}
$$

where $Z_1^\perp(\omega_q) = -W_\perp\tilde{Z}(\omega_q) = -W_\perp[\tilde{Z}_r(\omega_q) + i\,\tilde{Z}_i(\omega_q)]$, and $\sum_q$ has been replaced by $\int\omega_q/\omega_0$. In Fig. 3, we show the growth rate of the impedance corresponding to a uniform wake function , where [8]

$$
\tilde{Z}(\omega_q) = \frac{1}{\omega_q} - i\pi\delta(\omega_q), \tag{30}
$$

and the growth rate of the impedance of the broad-band resonator model, where

$$\tilde{Z}(\omega_q) = \frac{1}{2\omega_q \tilde{z}\,[1 + i\,(1/\tilde{\omega} - \tilde{\omega})]}, \tag{31}$$

$Q = 1$, $\tilde{z} = \hat{z}/b$, $\tilde{\omega} = \omega_q/\omega_R$, $\omega_R = c/b$, and $W_\perp = -2c\hat{z}R_s/b^3$. Note that, impedances for the broad-band resonator model and the uniform-wake model give a similar dependence of the growth rates on χ_0 and χ_1 [cf. Fig. 3]. In the resonator model, a longer bunch would scale down the growth rate of the HT instability. In the uniform-wake model, the growth rate is independent of σ_z. To illustrate the effectiveness of damping mechanism due to χ_1, we will employ Eq. (30) as the function of impedance in the following analysis and simulations.

Note that, $1/\tau_s^{(l)} = 0$, when $\chi_0 = 0$, since $\tilde{Z}_r(\omega_q)$ is odd in ω_q. As emphasized, the AC part of chromaticity alone does not cause the HT instability. The growth rate for the uniform-wake impedance can be approximated as,

$$\begin{aligned} 1/\tau_s^{(l)} &\approx \frac{16\Upsilon\chi_0}{\pi} J_0^2(\frac{\chi_1}{4}) \int_0^\infty \frac{d\chi_q}{\chi_q} J_l(\chi_q) J_l'(\chi_q) \\ &\approx \frac{32\Upsilon\chi_0}{\pi^2(4l^2-1)} J_0^2(\frac{\chi_1}{4}) \end{aligned} \tag{32}$$

up to the first order of χ_0, where the terms of $m \neq 0$ in $G_q^{(l)}$ [cf. Eq. (26)] are ignored. The growth rate is obviously decreased by the AC amplitude χ_1. When $\chi_1 = 0$, Eq. (32) reduces to the well-known [3,8] formula $1/\tau_s^{(l)} = 32\Upsilon\chi_0/\pi^2(4l^2-1)$.

C. Radial Modes

When considering realistic particle distributions, the radial eigenfunctions $R_l(r_z)$ are no longer degenerate. In this section, we assume a Gaussian longitudinal distribution, i.e.

$$\psi_{0z}(r_z) = \frac{N\eta c}{2\pi\sigma_z^2\omega_s} e^{-r_z^2/2\sigma_z^2} \tag{33}$$

and that the mode frequency shift $\Delta\Omega^{(l)}$ is smaller than ω_s, so that the modes $\Omega^{(l)}$ do not couple. The issues of azimuthal mode coupling will be briefly discussed later. The eigenmode equation, for the uncoupled lth mode, is a modified form of Sacherer's integral equation,

$$\begin{aligned} &\left(\frac{\Omega^{(l)} - \omega_{\beta 0}}{\omega_s} - l\right) R_l(r_z) \\ &= W(r_z) \int_0^\infty dr_z' r_z' R_l(r_z') K_l(r_z, r_z'), \end{aligned} \tag{34}$$

where

$$W(r_z) = \frac{\omega_s}{N\eta c}\psi_{0z}(r_z) = \frac{1}{2\pi\sigma_z^2} e^{-r_z^2/2\sigma_z^2}, \tag{35}$$

and the kernel of the integral equation is given by

$$\begin{aligned} K_l(r_z, r_z') = -i\frac{8\Upsilon}{T_0} \sum_q \tilde{Z}(\omega_q) \times \\ G_q^{(l)}\left(\frac{\omega_{\xi 1}}{4c} r_z, \frac{\omega_q - \omega_{\xi 0}}{c} r_z\right) \times \\ G_q^{(l)*}\left(\frac{\omega_{\xi 1}}{4c} r_z', \frac{\omega_q - \omega_{\xi 0}}{c} r_z'\right). \end{aligned} \tag{36}$$

Introducing an orthonormal complete set $\mathrm{e}_k^{(l)}(r_z)$ defined by

$$\int_0^\infty dr_z r_z W(r_z) \mathrm{e}_k^{(l)}(r_z) \mathrm{e}_{k'}^{(l)}(r_z) = \delta_{kk'}, \tag{37}$$

the eigenfunction can be expanded as

$$R_l(r_z) = W(r_z)\sum_{k=0}^{\infty} a_k \mathrm{e}_k^{(l)}(r_z). \tag{38}$$

For a Gaussian unperturbed distribution the weight function $W(r_z)$ [cf. Eq. (35)] has the orthonormal basis $\mathrm{e}_k^{(l)}(r_z)$ given by [13]

$$\mathrm{e}_k^{(l)}(r_z) = \frac{\sqrt{2\pi k!}}{(l+k)!}\left(\frac{r_z}{\sqrt{2}\sigma_z}\right)^l L_k^{(l)}\left(\frac{r_z^2}{2\sigma_z^2}\right), \tag{39}$$

where $L_k^{(l)}$ are the Laguerre polynomials. We now apply

$$\int_0^{\infty} dr_z r_z \mathrm{e}_k^{(l)}(r_z) \tag{40}$$

to both sides of Eq. (34). The integral equation becomes an eigenvalue system,

$$\left|\left(\frac{\Omega^{(l)} - \omega_{\beta 0}}{\omega_s} - l\right)\mathbf{I} - \mathbf{M}^{(l)}\right| = 0, \tag{41}$$

where $\mathbf{I}$ is an identity matrix,

$$\mathbf{M}_{kk'}^{(l)} = -i\frac{8\Upsilon}{T_0}\sum_q \tilde{Z}(\omega_q) \times g_{lk}(\omega_{\xi 1}, \omega_q - \omega_{\xi 0}) g_{lk'}^*(\omega_{\xi 1}, \omega_q - \omega_{\xi 0}), \tag{42}$$

and

$$g_{lk}(\omega_{\xi 1}, \omega_q - \omega_{\xi 0}) = \int_0^{\infty} dr_z r_z W(r_z) \mathrm{e}_k^{(l)}(r_z) G_q^{(l)}\left(\frac{\omega_{\xi 1}}{4c} r_z, \frac{\omega_q - \omega_{\xi 0}}{c} r_z\right). \tag{43}$$

Note that the meaning of g_{lk} is related to the beam frequency spectrum of the lth mode, since [cf. Eqs. (25), (26), and (43)]

$$\tilde{\rho}_1(\omega_q) = 2\pi\frac{\omega_s}{c\eta}\sum_l\sum_{k=0} i^{-l}\alpha_l a_k g_{lk}(\omega_{\xi 1}, \omega_q - \omega_{\xi 0}). \tag{44}$$

The eigenvalues then need to be solved by diagonalization of the infinite dimensional matrix $\mathbf{M}^{(l)}$. Note that, the number of azimuthal and radial nodes in the longitudinal phase space are, l and j, respectively. To achieve a qualitative description of the eigenmodes, we now focus only on the dominant radial mode, where $k = j = 0$. Using Eqs. (26), (35), and (39), for the integral in Eq. (43), in which $L_0^{(l)}(x^2) = 1$, we have [13], for the $(lj) = (l0)$ mode,

$$g_{l0}(x_1, x_q - x_0) = \frac{1}{\sqrt{2\pi l!}}\sum_{m=0}(2-\delta_{m0})\left(-i\frac{x_1}{4}\right)^m \frac{(x_q - x_0)^{2m+l}}{(2m+l)!} \times \sum_{q=0}(-1)^q \frac{\Gamma(q+l+3m/2+1)}{q!\Gamma(q+m+1)}\left(\frac{x_1}{4}\right)^{2q} \times {}_2F_1\left[-q, -m-q; 2m+l+1; \left(\frac{x_q - x_0}{x_1/4}\right)^2\right], \tag{45}$$

where $x_{(0,1)} = \omega_{\xi(0,1)}\sigma_z/\sqrt{2}c$, $x_q = \omega_q\sigma_z/\sqrt{2}c$, δ_{m0} is the Kronecker delta, and ${}_2F_1(a, b; c; x)$ is the hypergeometric function. Note that $x_{(0,1,q)} = \chi_{(0,1,q)}/\sqrt{2}$. The beam spectra $|g_{l0}(\chi_q)|^2$ are shown in Figs. 4. It can be seen that, the center of spectra is shifted by an amount of χ_0; and with a large enough χ_1, the spectral amplitudes are suppressed

for all azimuthal modes. This implies that, besides the additional incoherent tune spread due to χ_1 which causes more Landau damping [cf. Eq. (6)], the HT instability induced by χ_0 is further suppressed by χ_1, although the later effect is much less effective than the first one, as will be seen in the next section.

The beam spectrum $g_{l0}(0, \chi_q - \chi_0)$ reduces to the spectrum of the DC case when $\xi_1 = 0$:

$$g_{l0}(\chi_q - \chi_0) = \frac{1}{\sqrt{2\pi l!}\, 2^{l/2}} (\chi_q - \chi_0)^l e^{-(\chi_q - \chi_0)^2/2}. \tag{46}$$

The mode frequency can now be approximated for the dominant radial mode of a Gaussian beam, as

$$\Omega^{(l)} - \omega_{\beta 0} - l\omega_s \simeq -i \frac{8\Upsilon\omega_s}{T_0} N_g^{(l)} \tilde{Z}_{\rm eff}^{(l)}, \tag{47}$$

where

$$N_g^{(l)} = \sum_q |g_{l0}(\chi_1, \chi_q - \chi_0)|^2 \tag{48}$$

and the effective impedance is

$$\tilde{Z}_{\rm eff}^{(l)} = \left[N_g^{(l)}\right]^{-1} \sum_q \tilde{Z}(\omega_q) \, |g_{l0}(\chi_1, \chi_q - \chi_0)|^2 . \tag{49}$$

When $\chi_1 < 1$, one can approximate the beam spectrum by

$$\begin{aligned} &|g_{l0}(\chi_1, \chi_q - \chi_0)|^2 \\ &\approx \frac{1}{2\pi l!\, 2^l} (\chi_q - \chi_0)^{2l} e^{-(\chi_q - \chi_0)^2} J_0^2\left(\frac{\chi_1}{4}\right). \end{aligned} \tag{50}$$

For simplicity, instead of using the exact representation of the beam spectrum shown in Eq. (45), we use the approximate form of Eq. (50) in the following study, for the case of $\chi_1 < 1$. In this way, for a broad-band impedance, the growth rate per synchrotron period is simply

$$\begin{aligned} 1/\tau_s^{(l)} &\simeq -8\Upsilon \int d\omega_q \tilde{Z}_r(\omega_q) \, |g_{l0}(\chi_1, \chi_q - \chi_0)|^2 \\ &= -8\Upsilon N_l \Re\left[\tilde{Z}_{\rm eff}^{(l)}\right], \end{aligned} \tag{51}$$

where for a Gaussian beam,

$$N_l = \int d\omega_q \, |g_{l0}|^2 \approx \frac{\Gamma(l + 1/2)}{\pi\, l!\, 2^{l+1}} \frac{c}{\sigma_z} J_0^2\left(\frac{\chi_1}{4}\right). \tag{52}$$

The coherent tune shift is given by the real part of the mode frequency. For of a uniform-wake impedance [cf. Eq. (30)], we have

$$2\pi \Re[\Delta\nu^{(l)}] = -\frac{4\Upsilon}{l!\, 2^l} \nu_s \chi_0^{2l} e^{-\chi_0^2} J_0^2\left(\frac{\chi_1}{4}\right), \tag{53}$$

where $\Delta\nu^{(l)} = (\Omega^{(l)} - \omega_{\beta 0})/\omega_0 - l\,\nu_s$; and the growth rates of the two fundamental modes are approximately,

$$1/\tau_s^{(0)} \approx -4\Upsilon \mathrm{Erfi}\,(\chi_0)\, e^{-\chi_0^2} J_0^2\left(\frac{\chi_1}{4}\right), \tag{54}$$

and

$$1/\tau_s^{(1)} \approx \sqrt{\pi}\Upsilon\chi_0 L_{1/2}^{(-1/2)}(\chi_0^2)\, e^{-\chi_0^2} J_0^2\left(\frac{\chi_1}{4}\right), \tag{55}$$

where $1/\tau_s^{(l)} = 2\pi\Im[\Delta\nu^{(l)}]/\nu_s$, $\mathrm{Erfi}(x) = -i\,\mathrm{Erf}(ix)$, and $\mathrm{Erf}(x)$ is the error function. Fig. 5 show the real part and imaginary parts of the coherent tune shifts for $l = 0 \,\&\, l = 1$. When $\chi_0 \ll 1$, the growth rates can be further approximated by using $\mathrm{Erf}(\chi_0) \approx 2\chi_0/\sqrt{\pi}$, $L_{1/2}^{(-1/2)}(\chi_0^2) \approx 2/\pi$. For a uniform-wake impedance, and $\chi_1 < 1$, we recapitulate the growth rates in Table 1, when $\chi_0 \ll 1$.

	$\left[\tau_s^{(l)}\chi_0\Upsilon J_0^2(\chi_1/4)\right]^{-1}$	
	hollow	Gaussian
$l=0$	-3.242	-4.514
$l=1$	1.081	1.128

Table 1: Comparisons of the geometric factor of the growth rate of the HT instability, for a bunched beam with a hollow distribution and with a Gaussian distribution, when $\chi_0 \ll 1$. A uniform-wake impedance is assumed, and the effect of Landau damping in not included.

Simulations agree very well with Eq. (54) for the damping and growth rates of the $l=0$ mode of a Gaussian beam. Figs. (6) show examples of the bunch centroid motion of a Gaussian beam, where the evolution of the envelope agrees very well with the theory's prediction. In other words, the imaginary part of the coherent tune shift calculated is confirmed by simulations.

When the SHT effect is prominent, i.e. Υ is close to 1, the azimuthal mode-coupling is likely to occur. Examination of Eqs. (53), (54) and (55), shows that, both the real and imaginary parts of the coherent tune shift of the $(l0)$ mode are approximately reduced by $J_0^2(\chi_1/4)$. Even before solving the matrix of infinite dimension, or including the Landau damping, this suggests that the SHT threshold can be raised by a large value of χ_1.

The most important results in this section are Eqs. (53), (54) and (55), which are the real part and the imaginary part of the tune shift of a Gaussian beam with the model impedance of Eq. (30). These results will be used in the next section.

III. LANDAU DAMPING

In this section, we include in the linearized Vlasov analysis the incoherent tune spread induced by the varying chromaticity. We present an approximate stability criterion, a rigorous criterion using the dispersion relation, and comparisons with simulation results.

A. Approximate Stability Criterion

With the knowledge of the incoherent tune spread and coherent tune shift, which cause damping and instability respectively, we can now estimate a stability condition. Let's assume that the stability criterion for the HT instability is that the incoherent tune spread is larger than the absolute value of the coherent tune shift; that is

$$\sigma_\nu > \left|\Delta\nu^{(l)}\right|. \tag{56}$$

From Eqs. (6) and (47), a general expression for the stability condition is

$$\chi_1 > \frac{8}{\pi}\sqrt{\frac{2}{3}}\left(\frac{N_l}{g_\sigma}\right)\Upsilon\ \left|\tilde{Z}_{\rm eff}^{(l)}(\chi_0)\right|, \tag{57}$$

where the factor $J_0^2(\chi_1/4)$ is neglected. From Eqs. (47), (48), (50), and Figs. 4, one can see that, without taking into account Landau damping, χ_1 does not significantly reduce the coherent tune shift, unless $\chi_1 \gg 1$. Explicitly, the approximate stability criterion, expressed in terms of accelerator parameters, is

$$\xi_1 > c_l \frac{eI_0\left|Z_1^{\perp(l)}(\xi_0)\right|_{\rm eff}}{E}\left(\frac{R}{\sigma_z}\right)^2\left(\frac{\eta R}{\nu_s\nu_{\beta 0}^2}\right), \tag{58}$$

where $c_l = \sqrt{2/3}\Gamma(l+1/2)/\pi l! 2^{l+1}$ and the average current is $I_0 = Nec/C$. When $0<\chi_0<1$, the $l=1$ mode is usually the dominant unstable mode, and $c_1 = 0.058$. In contrast, when $-1<\chi_0<0$, the $l=0$ mode is the dominant unstable mode and $c_0 = 0.23$. Note that, as the dimensionality of $Z_1^\perp$ is [Ω/m], both sides of Eq. (58) are dimensionless.

As an example, consider a Gaussian beam distribution, an impedance function $\tilde{Z} = 1/\omega_q - i\pi\delta(\omega_q)$, and $\chi_0 = 0.2$, the stability criterion [cf. Eq. (57)] predicts that the $l=0$ mode is stabilized if $\chi_1 > \Upsilon$, and the $l=1$ mode is stabilized if $\chi_1 > 0.058\Upsilon$. In Figs. 7 and 8, we show the growth of the bunch centroid, rms-size, and rms-emittance

due to the HT instability, and its stabilization by various amounts of χ_1. The value of χ_1 needed to stabilize the bunch centroid motion is approximately consistent with the estimated criterion of Eq. (57). In Fig. 8, the bunch centroid motion is initially dominated by the $l = 0$ mode, which is a damping mode when $\chi_0 > 0$ [cf. Figs. 5 and 6]; the higher order unstable modes cause the growth of averaged bunch-center after the initial damping. The varying chromaticity, nonetheless, Landau damps all the higher order unstable modes when χ_1 is larger than the HT stability threshold estimated in Eq. (57).

Eq. (57) is an estimate for the stability condition, and is usually sufficient for the bunch centroid motion. A rigorous criterion may be derived by incorporating the incoherent tune spread in the Vlasov analysis. In doing so, one needs to include the damping mode by the method of singular eigenfunction expansion, and solve the dispersion relation [14]. The basic derivations are formulated in the next section.

B. Singular Eigenfunction Expansion

In this section, we use the method of singular eigenfunction expansion [14] to include the Landau damping in the Sacherer equation. We first rederive the betatron phase advance,

$$\begin{aligned}\Phi_\beta &= \int \frac{ds}{c}\omega_\beta(\delta) \\ &= \frac{\omega_{\beta 0}}{c}s + \frac{\omega_{\beta 0}}{c}\int ds\,\xi\,\delta = \phi_\beta + \Phi,\end{aligned} \tag{59}$$

where $\phi_\beta = \phi_y + S_1\phi_z\, r$,

$$\Phi = -\frac{\omega_{\xi 0}}{c}r\cos\phi_z - \frac{\omega_{\xi 1}}{4c}r\sin(2\phi_z), \tag{60}$$

$r_z \rightarrow r$, and $S_1 = \omega_{\xi 1}/2c$. The in-phase oscillation between the chromaticity modulation and the energy oscillation generates a tune spread proportional to $S_1\, r$, as illustrated in Sec. I. We now rewrite Eq. (34) as

$$R_l(r) = \frac{W(r)}{\nu_l - S_1 r}\int_0^\infty dr' r' R_l(r') K_l(r, r'), \tag{61}$$

where $\nu_l = (\Omega^{(l)} - \omega_{\beta 0})/\omega_s - l = \Delta\nu^{(l)}/\nu_s$, $\omega_{\beta 0} \rightarrow \omega_{\beta 0} + S_1\omega_s r$, and $\nu_l \rightarrow \nu_l - S_1 r$. According to the orthogonality condition defined in Eq. (37), the kernel $K_l(r, r')$ can be expanded as

$$K_l(r, r') = \sum_{k,k'} \mathbf{M}^{(l)}_{kk'}\mathbf{e}^{(l)}_k(r)\mathbf{e}^{(l)}_{k'}(r'), \tag{62}$$

where

$$\begin{aligned}\mathbf{M}^{(l)}_{kk'} = &\int_0^\infty dr\, r W(r)\mathbf{e}^{(l)}_k(r) \times \\ &\int_0^\infty dr' r' W(r')\mathbf{e}^{(l)}_{k'}(r') K_l(r, r').\end{aligned} \tag{63}$$

As in Sec. II, we now apply $\int dr r\mathbf{e}^{(l)}_j(r)$ on both sides of Eq. (61). The eigenvalue system becomes

$$\delta_{jk'} - \sum_k \alpha^{(l)}_{jk}\mathbf{M}^{(l)}_{kk'} = 0, \tag{64}$$

where

$$\alpha^{(l)}_{jk} = \int dr\, r\frac{\mathbf{e}^{(l)}_j(r)\mathbf{e}^{(l)}_k(r)W(r)}{\nu_l - S_1 r} = F_{jk}(\nu_l) + iG_{jk}(\nu_l), \tag{65}$$

$$F_{jk}(\hat{r}) = -\frac{1}{S_1}P.V.\int dr r\frac{\mathbf{e}^{(l)}_j(r)\mathbf{e}^{(l)}_k(r)W(r)}{r - \hat{r}}, \tag{66}$$

$$G_{jk}(\hat{r}) = -\frac{\pi}{S_1}\hat{r}\mathrm{e}_j^{(l)}(\hat{r})\mathrm{e}_k^{(l)}(\hat{r})W(\hat{r}), \tag{67}$$

$\hat{r} = \nu_l/S_1$, and *P.V.* is the Cauchy principal value. In Eq. (65), we have used the formula: $1/(r-\hat{r}) \rightarrow P.V./(r-\hat{r}) + i\pi\delta(\hat{r})$. The dispersion relation of the dominat radial mode is

$$\frac{1}{\alpha_{00}^{(l)}} = \mathbf{M}_{00}^{(l)}, \tag{68}$$

or, explicitly,

$$\begin{aligned} V + iU = \frac{i}{\alpha_{00}^{(l)}} &= \frac{i}{F_{00}(\nu_l) + iG_{00}(\nu_l)} \\ &= i\mathbf{M}_{00}^{(l)} \\ &= \frac{8\Upsilon}{2\pi} N_l \left\{ \Re\left[\tilde{Z}_{\mathrm{eff}}^{(l)}\right] + i\Im\left[\tilde{Z}_{\mathrm{eff}}^{(l)}\right] \right\}, \end{aligned} \tag{69}$$

where $V(U)$ is the real (imaginary) part of the $i/\alpha_{00}^{(l)}$, and $i/\alpha_{00}^{(l)}$ is the so called "beam transfer function" (BTF). For a Gaussian beam, we have

$$\begin{aligned} &\frac{i}{F_{00}(\nu_0) + iG_{00}(\nu_0)} = \\ &\frac{-i\chi_1^2/2}{\sqrt{2\pi}\chi_1 - 2\pi\nu_0 e^{-2\nu_0^2/\chi_1^2}\left[\mathrm{Erfi}\left(\frac{\sqrt{2}\nu_0}{\chi_1}\right) - i\right]}, \end{aligned} \tag{70}$$

and

$$\begin{aligned} &\frac{i}{F_{00}(\nu_1) + iG_{00}(\nu_1)} = \\ &\frac{-i\chi_1^4}{\sqrt{2\pi}\left(\chi_1^3 + 4\chi_1\nu_1^2\right) - 8\pi\nu_1^3 e^{-2\nu_1^2/\chi_1^2}\left[\mathrm{Erfi}\left(\frac{\sqrt{2}\nu_1}{\chi_1}\right) - i\right]}, \end{aligned} \tag{71}$$

for the $l = 0$ and $l = 1$ modes. The real and imaginary parts of the effective impedance are given by [cf. Eqs. (53), (54) and (55)]

$$\begin{aligned} &8\Upsilon N_l \Re\left[\tilde{Z}_{\mathrm{eff}}^{(l)}\right] = \\ &\begin{cases} 4\Upsilon \mathrm{Erfi}\left(\chi_0\right) e^{-\chi_0^2} J_0^2\left(\frac{\chi_1}{4}\right) & (l=0) \\ -\sqrt{\pi}\Upsilon\chi_0 L_{1/2}^{(-1/2)}(\chi_0^2)\, e^{-\chi_0^2} J_0^2\left(\frac{\chi_1}{4}\right) & (l=1) \end{cases}, \end{aligned} \tag{72}$$

$$8\Upsilon N_l \Im\left[\tilde{Z}_{\mathrm{eff}}^{(l)}\right] = -\frac{4\Upsilon}{l!\,2^l}\chi_0^{2l} e^{-\chi_0^2} J_0^2\left(\frac{\chi_1}{4}\right). \tag{73}$$

In Figs. 9 and 10, we show the stability diagrams in the $U - V$ space, when $l = 0\,\&l = 1$. The curve of the BTF (the outer limit on the $U - V$ plane), is determined by χ_1. The parameters related to the beam intensity and the effective impedance, i.e., Υ and χ_0 [cf. Eqs. (53), (54) & (55)], determine the curve of the inner elliptical circle on the $U - V$ plane. Note that, in drawing the figures, the contribution of $J_0^2(\chi_1/4)$ in the beam spectrum [cf. Eq. (50)] is moved to the left-hand side of the dispersion relation [cf. Eq. (69)].

We find that, the stability limit for the $l = 0$ mode is where $\nu_0 = 0$, i.e., $\Re(\mathrm{BTF}) = 0$. According to the dispersion relation [cf. Eq. (69)], the stability condition is $\Upsilon(l = 0) \leq 0.31\chi_1 e^{\chi_0^2}$. For the $l = 1$ mode, the stability limit is usually given by where $F_{00} = 0$, i.e. $\Im(\mathrm{BTF}) = 0$. Unlike the $l = 0$ mode, one needs to solve the dispersion relation numerically to obtain the stability condition of the $l = 1$ mode.

In short, it is the real (imaginary) part of the effective impedance that gives rise to the stability limit, for the $l = 1(l = 0)$ mode.

Figs. 11 and 12 show that the stability area can be enlarged by a larger χ_1, for both the $l = 0\,\&\,l = 1$ modes. Eqs. (70) and (71) show that the left-hand side of the dispersion relation is approximately proportional to χ_1; this implies that the SHT threshold can be enlarged by increasing χ_1.

The multiparticle simulations show that the rms-emittance of a Gaussian beam is stabilized when the the value of χ_1 approaches the stability threshold of Eq. (69) [cf. Figs. 13 and 14]. The results of simulation of the bunch centroid motion agree with the approximate stability limit, and the results of emittance growth agree with the exact stability criterion [cf. Fig. 15]. Compared with the rigorous criterion, to stabilize the bunch's higher moments, such as the rms-size and rms-emittance, χ_1 usually needs to be larger than the estimate from the approximate criterion [cf. Eq. (57)] by a factor of between 1 and 3.

As mentioned in previous sections, the varying chromaticity can not only stabilize the HT effect, but also increase the SHT threshold. Figs. 16 show the simulation results for the stabilization of the SHT instability by a sufficiently large χ_1, when $\Upsilon = 1.65$ and $\chi_0 = 0$. Note that the SHT stability threshold, without varying chromaticity, is approximately $\Upsilon < 1$ (which has been confirmed by simulations). This implies that the current limit in a storage ring can be increased by the varying chromaticity scheme.

The stability criterion derived in this section are in good agreement with the simulation results, and the criterion provides a useful guidance for the implementation of the varying chromaticity scheme.

IV. CONCLUSION

In summary, we have shown that, by the varying chromaticity scheme, the head-tail instability is suppressed and a stability threshold is developed. The underlying physical mechanism of the damping scheme is from the Landau damping due to an additional incoherent betatron tune spread induced by the varying chromaticity. Moreover, the varying part of chromaticity rotates the head-tail phase, such that the chromatic term is $\pm\pi/2$ out of phase from the resonant term, in the first and second half synchrotron period, respectively. The imaginary terms ($\pm\pi/2$ out of phase terms) are therefore cancelled out by varying chromaticity in one synchrotron period. Consequently, the AC part of the chromaticity does not cause instability. Multi-particle simulations confirmed the estimated Landau damping rate, the mode analysis, and the stability condition. In short, it is both the strong focusing principle and the Landau damping that make this scheme work. With large enough AC part of the chromaticity, one should be able to increase the threshold of the strong head-tail instability.

Studies of practical issues, such as rapidly modulated sextupole magnets and the reduction of dynamic apertures; and further theoretical works, such as exact calculations of the azimuthal mode-coupling, are required. Also, of course, the practical aspects of varying chromaticity must be compared with the other schemes that also introduce an incoherent tune spread, e.g., space-charge, ion-trapping, rf-nonlinearity, and octupole magnets.

Finally, this work suggests that temporal variation of accelerator parameters might be useful in the control of other instabilities.

V. ACKNOWLEDGMENTS

We are grateful to Sasha A. Zholents, who called our attention to the paper by Nakamura. We alo thank Alexander W. Chao for his helpful discussion. In particular, W.-H. C. would like to thank Robert L. Gluckstern for his introduction of the concept of Alternating-Phase-Focusing (APF) which inspired the early idea of this work.

APPENDIX A: MULTI-PARTICLE SIMULATION

A simulation code has been developed to study the damping effect of the varying chromaticity for the HT instability. The code simulates a bunched beam traversing a ring with a transverse impedance. The momentum P_y is changed by the kick of the transverse wake force, where $P_y = (c/\omega_{\beta 0})y'$. Particle's betatron oscillation is carried out by a rotation matrix, where Eqs. (1) and (2) are used for the angular frequency. A uniform transverse wake function is used. No longitudinal wake force is included. Eqs. (7) and (10) are transformed into a 4-D map for particle's transverse and longitudinal motions.

The parameters used in the simulations are listed in Table 2.

Particle's classical radius r_0[cm]	1.534×10^{-16}
Energy E[GeV]	40
Circumference C[m]	6400
Slippage factor η	10^{-3}
Synchrotron tune ν_s	0.0094
Betatron tune $\nu_{\beta 0}$	16.35
RMS bunch length σ_z[cm]	1
RMS bunch size σ_y[cm]	0.1
Shunt impedance $R_s[\Omega]$	3000
Pipe radius b[cm]	3.0
Chromaticity(Head-tail phase) $\xi_0(\chi_0)$	1.246(0.2)
Initial beam transverse offset Δy[cm]	0.1
Number of particles per bunch N	2×10^{11}

Table 2: Parameters used in the simulations. Note that, from this table, the intensity parameter is $\Upsilon = 0.22$.

The accelerator parameters can be scaled according to the three dynamical parameters Υ, χ_0, and χ_1, which are the only parameters relevant to the dynamics discussed. In simulations, a bunch beam is loaded with a bi-Gaussian distribution in both the longitudinal and transverse phase spaces. All results are numerically converged when the number of macro-particles simulated is larger than 400.

The curves of $\langle y \rangle$ and $y_{\rm rms}$ presented in this paper have been averaged over a synchrotron period, they are defined as

$$\langle y \rangle(\tau_n) = \left[\frac{1}{2N_s+1} \sum_{i=\tau_n-N_s}^{\tau_n+N_s} \bar{y}^2(i) \right]^{1/2}, \tag{A1}$$

$$y_{\rm rms}(\tau_n) = \left[\frac{1}{2N_s+1} \sum_{i=\tau_n-N_s}^{\tau_n+N_s} \sigma_y^2(i) \right]^{1/2}, \tag{A2}$$

where

$$\bar{y}(i) = \frac{1}{N_m} \sum_{m=1}^{N_m} y_m(i),$$

$$\sigma_y^2(i) = \frac{1}{N_m} \sum_{m=1}^{N_m} \left[y_m(i) - \bar{y}(i) \right]^2, \tag{A3}$$

N_m is the number of macro-particles used in the simulations, τ_n is the number of turn, and N_s is the integer part of $1/\nu_s$. The rms-emittance is defined as

$$\varepsilon_{\rm rms}(\tau_n) = \sqrt{\sigma_y^2(\tau_n)\sigma_{P_y}^2(\tau_n) - \sigma_{y-P_y}^2(\tau_n)}, \tag{A4}$$

where

$$\sigma_{y-P_y}^2(\tau_n) = \frac{1}{N_m} \sum_{m=1}^{N_m} \left[y_m(\tau_n) - \bar{y}(\tau_n) \right] \left[P_{ym}(\tau_n) - \bar{P}_y(\tau_n) \right]. \tag{A5}$$

APPENDIX B: PERIODICITY OF VARYING CHROMATICITY

In this appendix, by using a two-particle model, we show that the periodicity of chromaticity modulation n must be an odd number, such that the AC part of the chromaticity does not cause additional HT instability.

For a two macro-particle system, the longitudinal motion of the two macro-particles is prescribed as:

$$z_{1,2} = \pm\hat{z}\,\sin\phi, \quad \delta_{1,2} = -\frac{z'_{1,2}}{\eta} = \mp\frac{\omega_s\hat{z}}{c\eta}\,\cos\phi, \tag{B1}$$

where $\hat{z}$ is the oscillation amplitude with respect to the bunch center, and the upper (lower) sign denotes for the 1st (2nd) particle. The transverse motion in the first half synchrotron period, i.e. $0 < s/c < T_s/2$, can be described as follows,

$$y_1'' + \frac{\omega_\beta^2(\delta_1)}{c^2}y_1 = 0, \tag{B2}$$

$$y_2'' + \frac{\omega_\beta^2(\delta_2)}{c^2}y_2 = -\frac{Nr_0}{2\gamma C}W_\perp\, y_1, \tag{B3}$$

where a constant short-range transverse wake $W_\perp$ is assumed. For the second half period, i.e. $T_s/2 < s/c < T_s$, $y_1 \leftrightarrow y_2$.

According to Eqs. (1), (2), and (B1), the betatron frequencies of the head and tail split as

$$\omega_{\beta 1,2}(s) = \omega_{\beta 0} \mp \omega_s \sum_{n=0} \chi_n \cos\phi\, \cos(n\phi + \theta_n). \tag{B4}$$

The approximate solution of Eqs. (B3) can be found by assuming

$$y_{1,2}(s) = Y_{1,2}(s)\, \exp\left[-i\Phi_{1,2}(s)\right] \tag{B5}$$

where both $Y(s)$ and $\Phi(s)$ vary slowly compared with the betatron oscillation,

$$\Phi_{1,2}(s) = \int_0^s ds' \frac{\omega_{\beta 1,2}(s')}{c} = \omega_{\beta 0}\frac{s}{c} \mp \frac{1}{2}\sum_{n=0} \chi_n\, g_n, \tag{B6}$$

and

$$\begin{aligned} g_n(n \neq 1) &= \cos\theta_n \left[\frac{\sin(n+1)\phi}{n+1} + \frac{\sin(n-1)\phi}{n-1}\right] \\ &+ \sin\theta_n \left[\frac{\cos(n+1)\phi - 1}{n+1} + \frac{\cos(n-1)\phi - 1}{n-1}\right], \end{aligned} \tag{B7}$$

$$g_1 = \cos\theta_1 \left(\frac{1}{2}\sin 2\phi + \phi\right) + \frac{1}{2}\sin\theta_1\,(\cos 2\phi - 1)\,. \tag{B8}$$

Substituting Eq. (B5) into Eq. (B3) and neglecting the small parts, where

$$(|Y_2''/Y_2|, |\Phi_2''|) \ll |\Phi_2' Y_2'/Y_2| \simeq \omega_{\beta 0} Y_2'/cY_2 \tag{B9}$$

and $\omega_s \ll \omega_{\beta 0}$, leads to

$$Y_2'(s) \simeq i2\frac{\omega_s}{c\pi}\Upsilon Y_1(0) \exp\left(i\sum_{n=0}\chi_n g_n\right). \tag{B10}$$

Integration of Eq. (B10) leads to

$$Y_2(cT_s/2) \simeq Y_2(0) + i2\Upsilon S_I Y_1(0), \tag{B11}$$

where

$$S_I = \frac{1}{\pi}\int_0^\pi d\phi \exp\left(i\sum_{n=0}\chi_n g_n\right). \tag{B12}$$

Similarly, for the second half synchrotron period, we have

$$Y_1(cT_s) \simeq Y_1(cT_s/2) + i2\Upsilon S_{II} Y_2(cT_s/2), \tag{B13}$$

where

$$S_{II} = \frac{1}{\pi}\int_{\pi}^{2\pi} d\phi \exp\left(-i\sum_{n=0}\chi_n h_n\right), \tag{B14}$$

and

$$\begin{aligned} h_n(n\neq 1) = \cos\theta_n &\left[\frac{\sin(n+1)\phi}{n+1} + \frac{\sin(n-1)\phi}{n-1}\right] + \\ &\sin\theta_n\left[\frac{\cos(n+1)\phi-(-1)^{n+1}}{n+1} + \right. \\ &\left.\frac{\cos(n-1)\phi-(-1)^{n-1}}{n-1}\right], \end{aligned} \tag{B15}$$

$$\begin{aligned} h_1 = \cos\theta_1 &\left(\frac{1}{2}\sin 2\phi + \phi - \pi\right) + \\ &\frac{1}{2}\sin\theta_1\left(\cos 2\phi - 1\right). \end{aligned} \tag{B16}$$

The amplitudes of the two-particle system after a complete synchrotron period can therefore be written as

$$\begin{aligned} \boldsymbol{V}(s/c = T_s) &= \boldsymbol{M}_{II}\cdot\boldsymbol{M}_I\cdot\boldsymbol{V}(s/c=0) \\ &= \boldsymbol{M}\cdot\boldsymbol{V}(0), \end{aligned} \tag{B17}$$

where $\boldsymbol{V} = (Y_1, Y_2)^T$, and the transfer map is

$$\begin{aligned} \boldsymbol{M} &= \begin{bmatrix} 1 & i2\Upsilon S_{II} \\ 0 & 1 \end{bmatrix}\cdot\begin{bmatrix} 1 & 0 \\ i2\Upsilon S_I & 1 \end{bmatrix} \\ &= \begin{bmatrix} 1-4\Upsilon^2 S_I S_{II} & i2\Upsilon S_{II} \\ i2\Upsilon S_I & 1 \end{bmatrix}. \end{aligned} \tag{B18}$$

The eigenvalues of $\boldsymbol{M}$ are

$$\lambda = 1 - 2\Upsilon^2 S \pm \sqrt{4\Upsilon^2 S\left(\Upsilon^2 S - 1\right)}, \tag{B19}$$

where $S = S_I S_{II}$. Note that when the chromaticity is constant, and the head-tail phase is small, i.e. $n = 0$ and $\chi_0 \ll 1$, we have $S_I = S_{II} \simeq 1 + 4i\chi_0/\pi$ [8]. When the chromaticity is zero, i.e. $\chi_0 = 0$, and $\Upsilon < 1$, the modulus of the eigenvalue is one and the system is stable. The value $\Upsilon = 1$ corresponds to the threshold of the SHT instability.

To investigate the stability of the two-particle system, we first discuss the situation when the head-tail phase is small, i.e. $\chi_n \ll 1$. The functions S_I, S_{II} can then be approximated as

$$S_I \approx 1 + i\sum_{n=0}\chi_n G_n, \tag{B20}$$

$$S_{II} \approx 1 - i\sum_{n=0}\chi_n H_n, \tag{B21}$$

where

$$\begin{aligned} G_n(n\neq 1) &= \int_0^{\pi} d\phi g_n(\phi) \\ &= \frac{1}{\pi}\cos\theta_n\left[\frac{1+(-1)^n}{(n+1)^2} + \frac{1+(-1)^n}{(n-1)^2}\right] \\ &\quad -\sin\theta_n\left(\frac{1}{n+1} + \frac{1}{n-1}\right), \end{aligned} \tag{B22}$$

$$\begin{aligned} H_n(n\neq 1) &= \int_{\pi}^{2\pi} d\phi h_n(\phi) \\ &= -\frac{1}{\pi}\cos\theta_n\left[\frac{1+(-1)^n}{(n+1)^2} + \frac{1+(-1)^n}{(n-1)^2}\right] \\ &\quad +\sin\theta_n\left[\frac{(-1)^n}{n+1} + \frac{(-1)^n)}{n-1}\right], \end{aligned} \tag{B23}$$

and

$$G_1 = H_1 = \frac{\pi}{2}\cos\theta_1 - \frac{1}{2}\sin\theta_1. \tag{B24}$$

The product of S_I and S_{II} in Eq. (B19) is then

$$\begin{aligned} S &= S_I S_{II} \\ &= 1 + \sum_{n,m=0} \chi_n \chi_m G_n H_m + i \sum_{n=0} \chi_n \left(G_n - H_n\right). \end{aligned} \tag{B25}$$

Note that, in Eqs. (B20) and (B21), the real part of $S_I(S_{II})$ is the resonant term, and the imaginary part is the chromatic term, in the 1st(2nd) half of a synchrotron period. Examining the form of the eigenvalue λ, the stability condition is, in general, when

$$S \in \Re, \;\; S > 0 \;\text{ and }\; \Upsilon^2 < 1/S, \tag{B26}$$

where the modulus of eigenvalue of the transfer map $\boldsymbol{M}$ equals to one, i.e. $|\lambda| = 1$. Since $G_n - H_n = 0$ when

$$n \subset odd, \tag{B27}$$

or

$$n \subset even \;\;\&\;\; \theta_n = \tan^{-1}\left[\frac{2(n^2+1)}{\pi n(n^2-1)}\right], \tag{B28}$$

which makes the imaginary part of S vanishes, we conclude that the stability conditions of the had-tail instability with varying chromaticity when $\chi_n \ll 1$, are Eqs. (B26)-(B28). Note that in case the chromaticity is a constant, i.e. when $n = 0$ only, we have $G_0 - H_0 = 8/\pi$, $\Im(S) \neq 0$, and $|\lambda| \neq 1$, the two-particle system is inherently unstable.

In other words, for a small head-tail phase χ_n, using a varying chromaticity with an odd function of synchrotron oscillation period, one can build up a stability threshold for Υ from zero to $1/\sqrt{S}$. An odd chromaticity function can be achieved, by either alternating the sign of ξ or modulating ξ by a sinusoidal function within a synchrotron period.

---

[1] W.-H. Cheng, A. M. Sessler, and J. S. Wurtele, (submitted for publication), Lawrence Berkeley National Laboratory Report, LBNL-39642 (1996).

[2] The SPEAR Group, *Proc. 9th Int. Conf. High Energy Accel.*, SLAC, 1974, p.338; J. Gareyte & F. Sacherer, *Proc. 9th Int. Conf. High Energy Accel.*, SLAC, 1974, p.341; Y. Miyahara & K. Takata, Part. Accel. **10**, 125 (1980).

[3] C. Pellegrini, Nuovo Cimento **64A**, 447 (1969); M. Sands, SLAC Reports TN-69-8 and TN-69-10 (1969); F. Sacherer, *Proc. 9th Int. Conf. High Energy Accel.*, SLAC, 1974, p.347.

[4] R. H. Siemann, *AIP Proc.* **127**, Phys. High Energy Part. Accel., BNL/SUNY, 1983, p.368; R. H. Siemann, Nucl. Instr. Meth. **221**, 293 (1984).

[5] E. Gianfelice, DESY-HERA 94-3, p.25, (1994); F. Galluccio, Part. Accel. **50**, 141 (1995).

[6] R. Cappi, Part. Accel. **28**, 117 (1995).

[7] E. Kikutani, Part. Accel. **52**, 251 (1996).

[8] A. W. Chao, *Physics of Collective Instabilities in High Energy Accelerators*, (John Wiley & Sons, New York, 1993).

[9] K. Johnsen, *Proc. CERN Symposium on High Energy Accel. and Pion Phys.*, Geneva, 1956, Vol. 1, p.106; K. Takayama, Part. Accel. **14**, 201 (1984); S. Y. Lee & J. M. Wang, IEEE Trans. Nucl. Sci. **NS-32**, 2323 (1985); J. Wei & S. Y. Lee, Part. Accel. **28**, 77 (1990).

[10] T. Nakamura, *Proc. 1995 IEEE Part. Accel. Conf.*, Vol. 5, 1995, p.3100.

[11] D. Robin *et al.*, Phys. Rev. E, **48**, 3, p.2149,(1993); A. Amiry *et al.*, Part. Accel., **44**, 57, (1994).

[12] D. Boussard, CERN Lab II/RF/Int 75-2 (1975).

[13] I. S. Gradshteyn and I.M. Ryzhik, *Table of Integrals, Series, and Products*, (Academic, San Diego, 1994), 5th ed., p. 739.

[14] L. D. Landau, J. Phys. U.S.S.R., **10**, 25 (1946); N. G. van Kampen, Physica, **21**, 949, (1955); F. J. Sacherer, CERN/SI-BR/72-5, 1972; Y. Chin, K. Satoh and K. Yokoya, Part. Accel., **13**, 45, (1983).

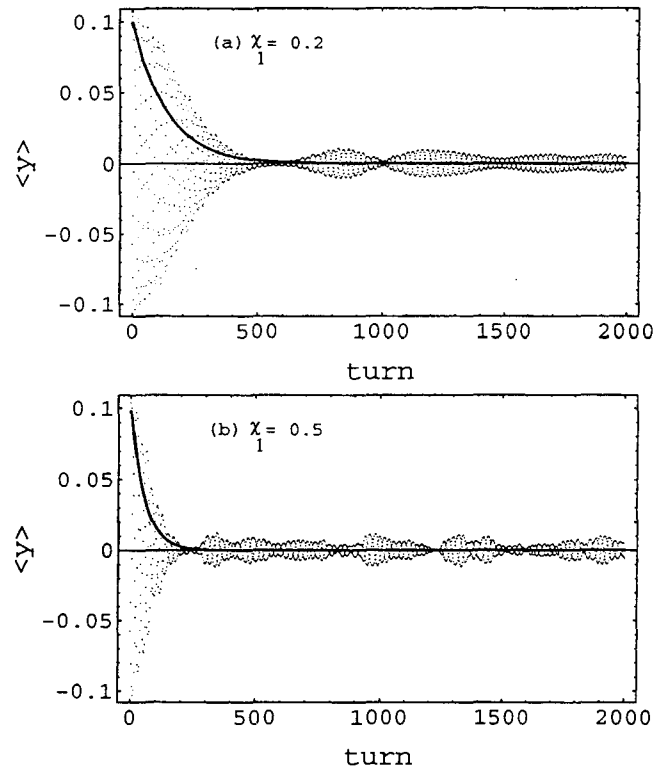

FIG. 1. Multi-particle simulation results showing damping of the centroid motion of a Gaussian beam, when $\Upsilon = 0.11$, $\chi_0 = 0$, (a) $\chi_1 = 0.2$, and (b) $\chi_1 = 0.5$. The solid lines are where, according to Eq. (6), $\langle y \rangle[\text{turn}] = 0.1 \exp(-\text{turn}/\tau_{LD})$. See Eqs. (8) and (9) for definitions of χ_0, χ_1, and Υ.

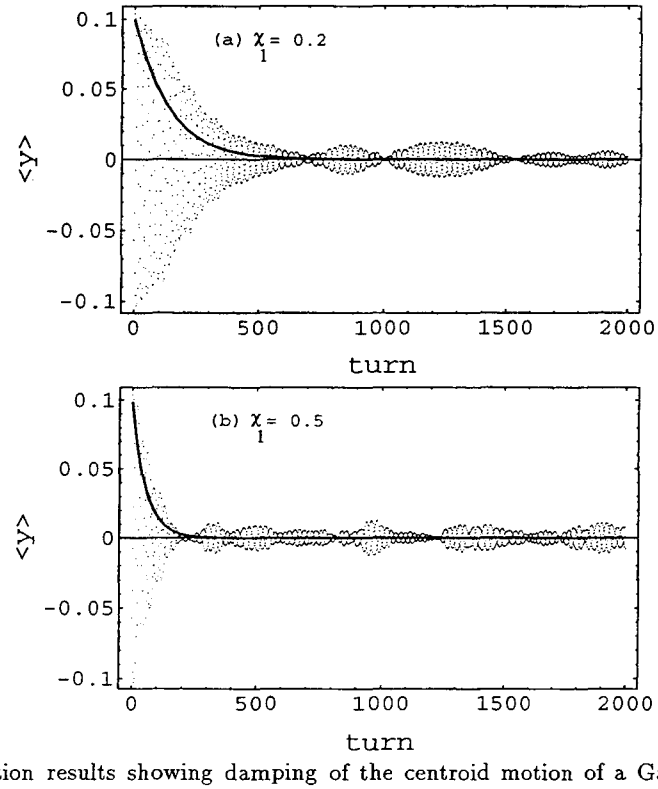

FIG. 2. Multi-particle simulation results showing damping of the centroid motion of a Gaussian beam, when $\Upsilon = 0.328$, $\chi_0 = 0$, (a) $\chi_1 = 0.2$, and (b) $\chi_1 = 0.5$. The solid lines are where, according to Eq. (6), $\langle y \rangle[\text{turn}] = 0.1 \exp(-\text{turn}/\tau_{LD})$. See Eqs. (8) and (9) for definitions of χ_0, χ_1, and Υ.

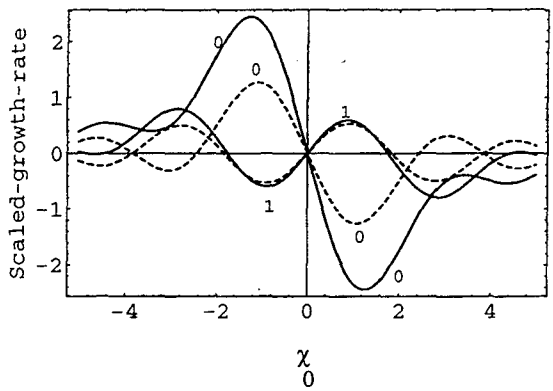

FIG. 3. Scaled growth rate, $1/\tau_s^{(l)}/\Upsilon$, of a hollow beam due to the impedances of a uniform-wake (solid line) and a broad-band resonator model (dashed line), when $\chi_1 = 0$, $\tilde{z} = 0.1$. Curves are labeled by the azimuthal mode index l. See Eqs. (8) and (9) for definitions of χ_0, χ_1, and Υ.

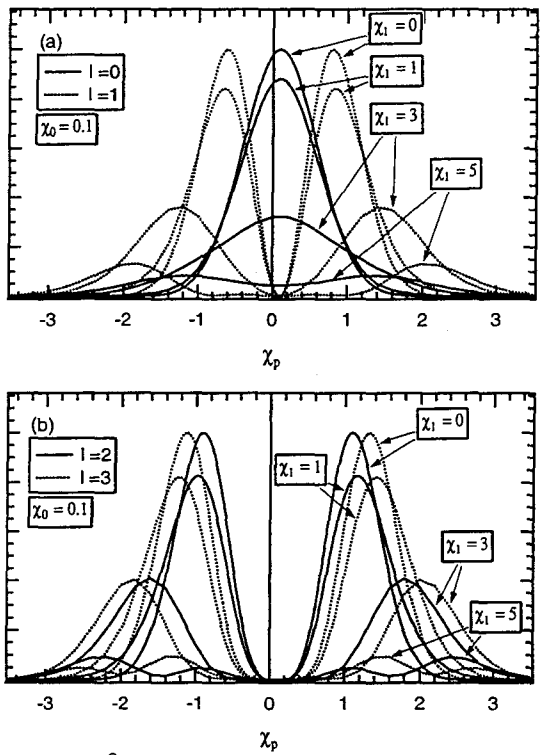

FIG. 4. Normalized frequency spectra $|g_{l0}(\chi_q)|^2$ of a Gaussian beam, when $\chi_0 = 0.1$, (a) $l = 0\,\&\,1$, and (b) $l = 2\,\&\,3$. See Eq. (8) for definition of χ_0 and χ_1.

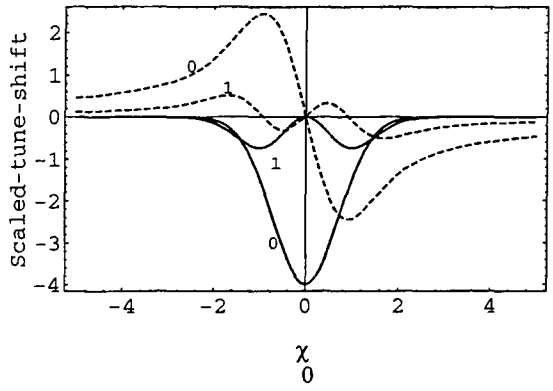

FIG. 5. Scaled coherent tune shift of a Gaussian beam due to the impedance of Eq. (30) vs. χ_0, when $\chi_1 = 0$, and where the solid(dashed) lines are the real(imaginary) part of $2\pi\Delta\nu^{(l)}/\nu_s\Upsilon$. Curves are labeled by the azimuthal mode index l. See Eqs. (8) and (9) for definitions of χ_0, χ_1, and Υ.

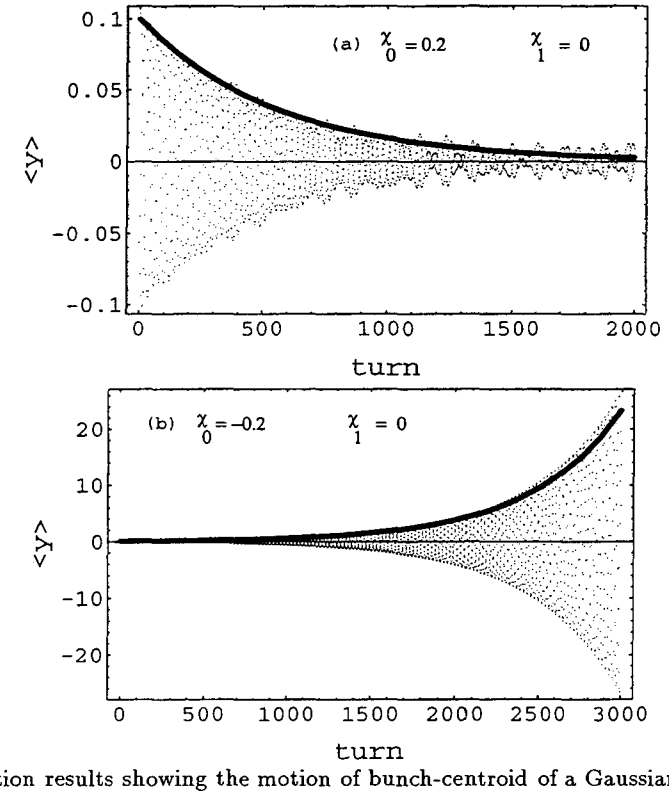

FIG. 6. Multi-particle simulation results showing the motion of bunch-centroid of a Gaussian beam, when $\chi_1 = 0$, $\Upsilon = 0.22$, (a) $\chi_0 = +0.2$, and (b) $\chi_0 = -0.2$. The solid lines are where, according to Eq. (54), $\langle y\rangle[\text{turn}] = 0.1\exp(\nu_s \text{turn}/\tau_s^{(0)})$. See Eqs. (8) and (9) for definitions of χ_0, χ_1, and Υ.

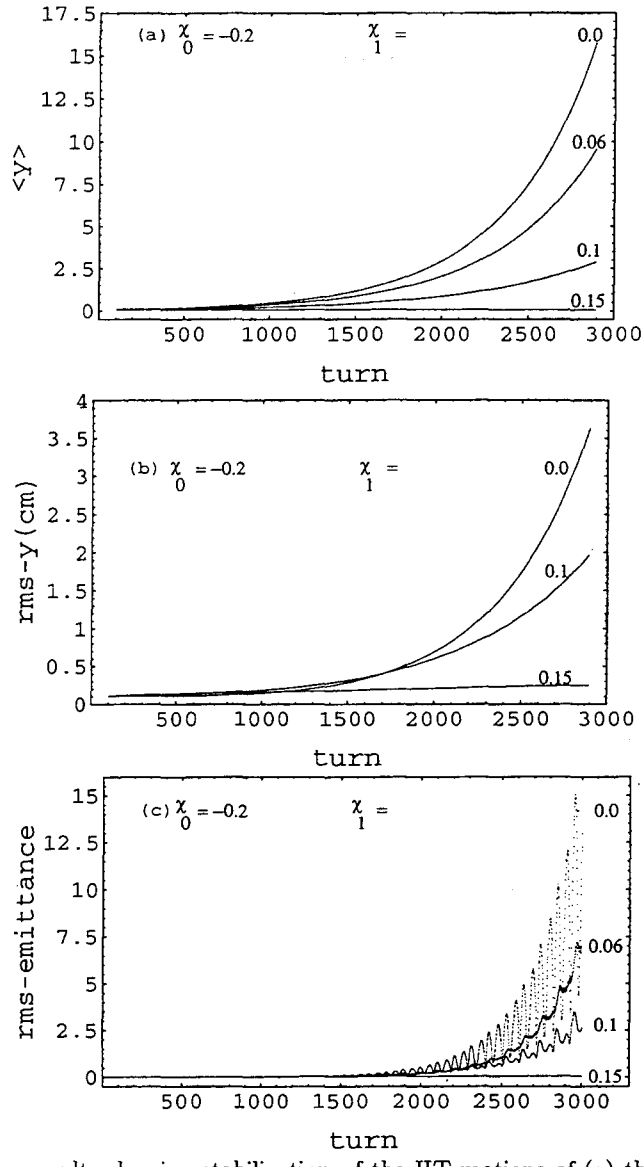

FIG. 7. Multi-particle simulation results showing stabilization of the HT motions of (a) the centroid, (b) the rms-size, and (c) the rms-emittance of a Gaussian beam by χ_1, when $\chi_0 = -0.2$ and $\Upsilon = 0.22$. The estimated stability threshold for the $l = 0$ mode, according to Eq. (57), is $\chi_1 \geq 0.22$. See Eqs. (8) and (9) for definitions of χ_0, χ_1, and Υ.

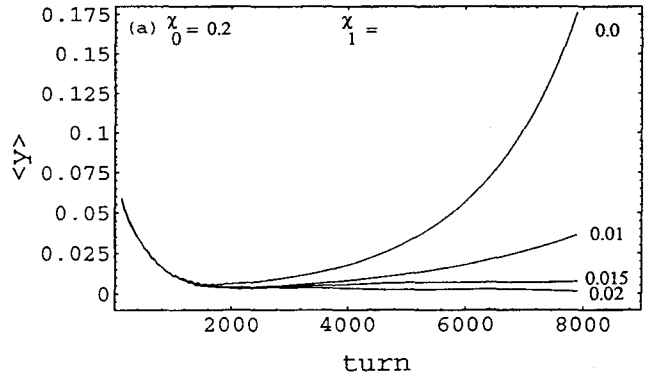

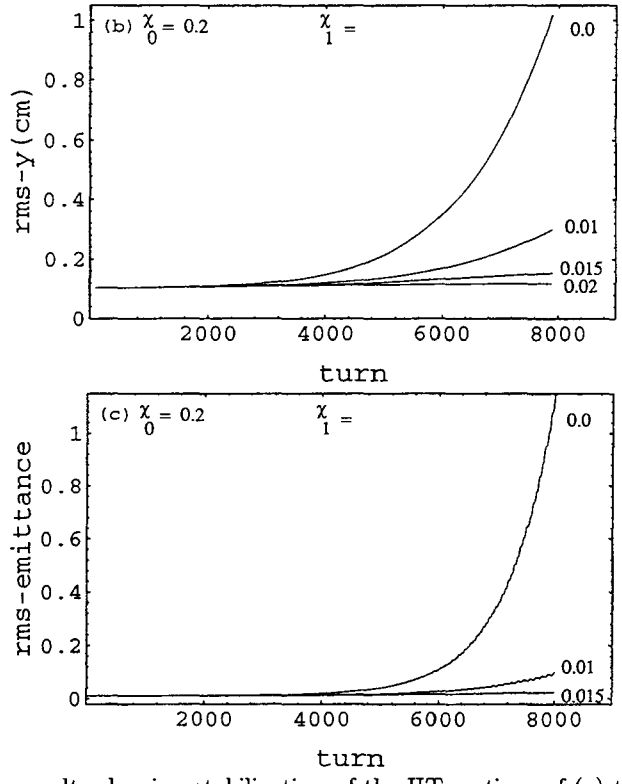

FIG. 8. Multi-particle simulation results showing stabilization of the HT motions of (a) the centroid, (b) the rms-size, and (c) the rms-emittance of a Gaussian beam by χ_1, when $\chi_0 = 0.2$ and $\Upsilon = 0.22$. The estimated stability threshold for the $l = 1$ mode, according to Eq. (57), is $\chi_1 \geq 0.0127$. See Eqs. (8) and (9) for definitions of χ_0, χ_1, and Υ.

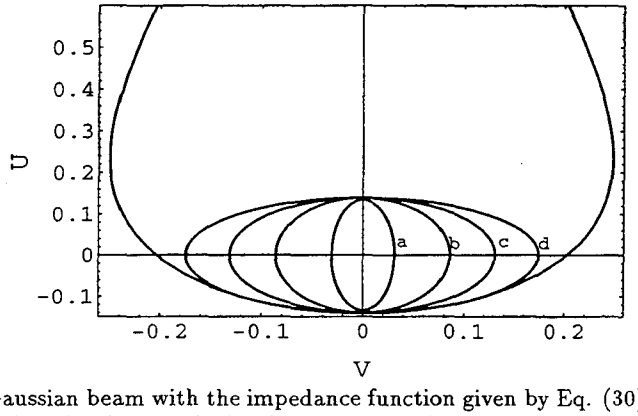

FIG. 9. Stability diagram of a Gaussian beam with the impedance function given by Eq. (30), for the $l = 0$ mode. Parameters that label the ellipses are: $(-\chi_0, \Upsilon)$ = (a) (0.2,0.22), (b) (0.5,0.28), (c) (0.7,0.36), (d) (0.85,0.45). The outer curve is where $\chi_1 = 0.7$. See Eqs. (8) and (9) for definitions of χ_0, χ_1, and Υ.

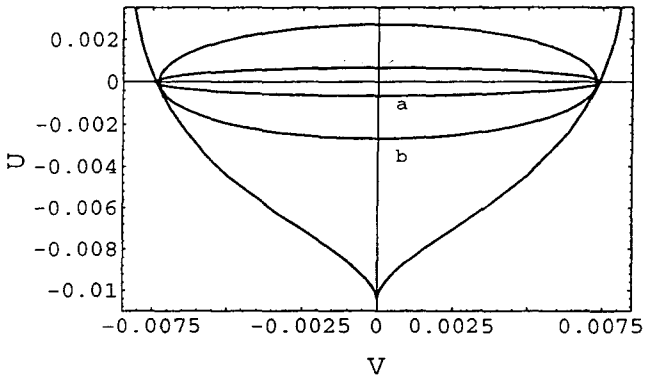

FIG. 10. Stability diagram of a Gaussian beam with the impedance function shown in Eq. (30), for the $l = 1$ mode. Parameters that label the ellipses are: $(\chi_0, \Upsilon) =$ (a) (0.05,0.83), (b) (0.2,0.22). The outer curve is where $\chi_1 = 0.026$. See Eqs. (8) and (9) for definitions of χ_0, χ_1, and Υ.

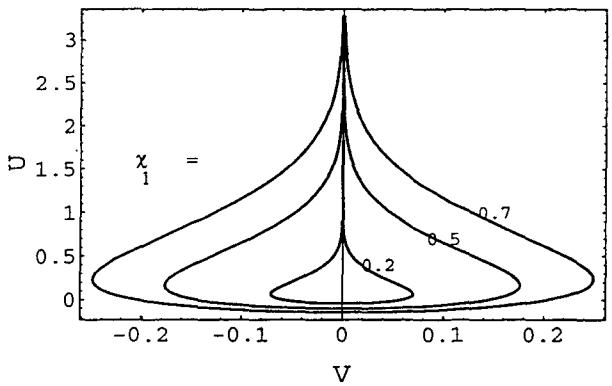

FIG. 11. Stability diagram of a Gaussian beam with the impedance function shown in Eq. (30), for the $l = 0$ mode. The stability boundaries are enlarged by χ_1. See Eqs. (8) and (9) for definitions of χ_0, χ_1, and Υ.

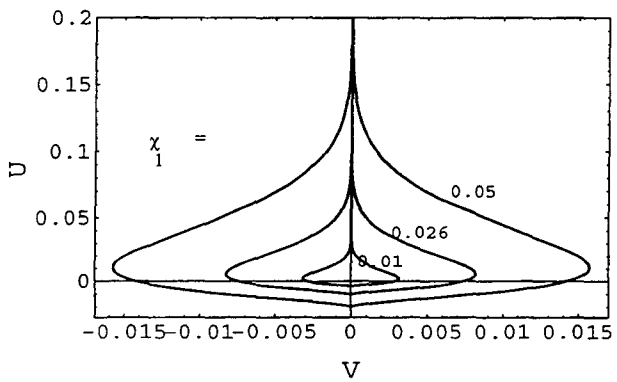

FIG. 12. Stability diagram of a Gaussian beam with the impedance function shown in Eq. (30), for the $l = 1$ mode. The stability boundaries are enlarged by χ_1. See Eqs. (8) and (9) for definitions of χ_0, χ_1, and Υ.

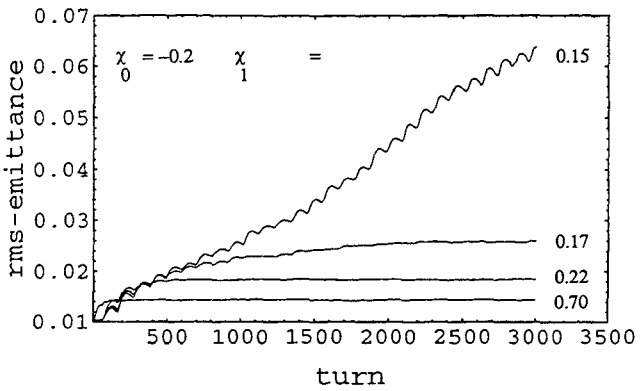

FIG. 13. Multi-particle simulation result showing stabilization of the HT motions of the rms-emittance of a Gaussian beam when $\chi_1 \to 0.7$ – the theoretical stability threshold of the $l = 0$ mode [cf. Eq. (69)]. Here $\chi_0 = -0.2$, $\Upsilon = 0.22$. See Eqs. (8) and (9) for definitions of χ_0, χ_1, and Υ.

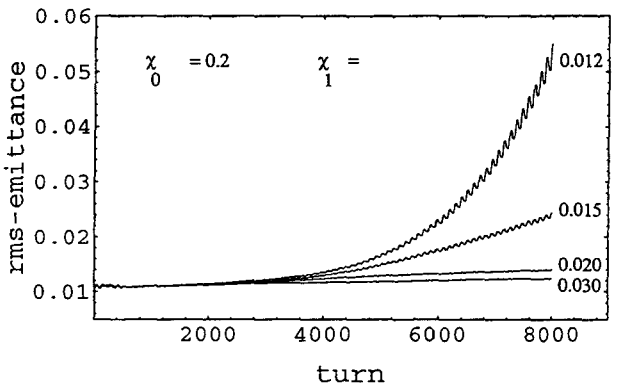

FIG. 14. Multi-particle simulation result showing stabilization of the HT motions of the rms-emittance of a Gaussian beam when $\chi_1 \to 0.026$ – the theoretical stability threshold of the $l = 1$ mode [cf. Eq. (69)]. Here $\chi_0 = 0.2$, $\Upsilon = 0.22$. See Eqs. (8) and (9) for definitions of χ_0, χ_1, and Υ.

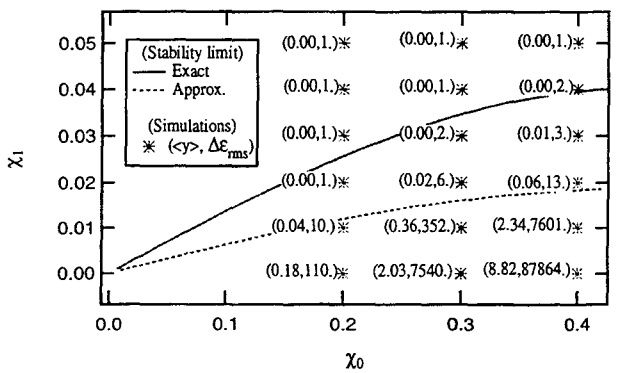

FIG. 15. Stability limits of a Gaussian beam with the impedance function of Eq. (30) for the $l = 1$ mode, in the AC (χ_1) vs. DC (χ_0) space. Here $\Upsilon = 0.22$, $\langle y \rangle$ is the averaged centroid motion at 8000 turns, $\Delta\epsilon\text{rms} = \epsilon\text{rms}(8000)/\epsilon\text{rms}(0)$, and the approximate and exact stable limits are plotted according to the criteria shown in Eqs. (57) and (69), respectively. The region below the solid (dashed) line is stable for the bunch's rms-emittance (centroid) motion. Note that, $\langle y \rangle(0) = 0.1$[cm], $\epsilon\text{rms}(0) = 0.01$[cm], and $\Delta\epsilon\text{rms}$ is rounded to the closest integer.

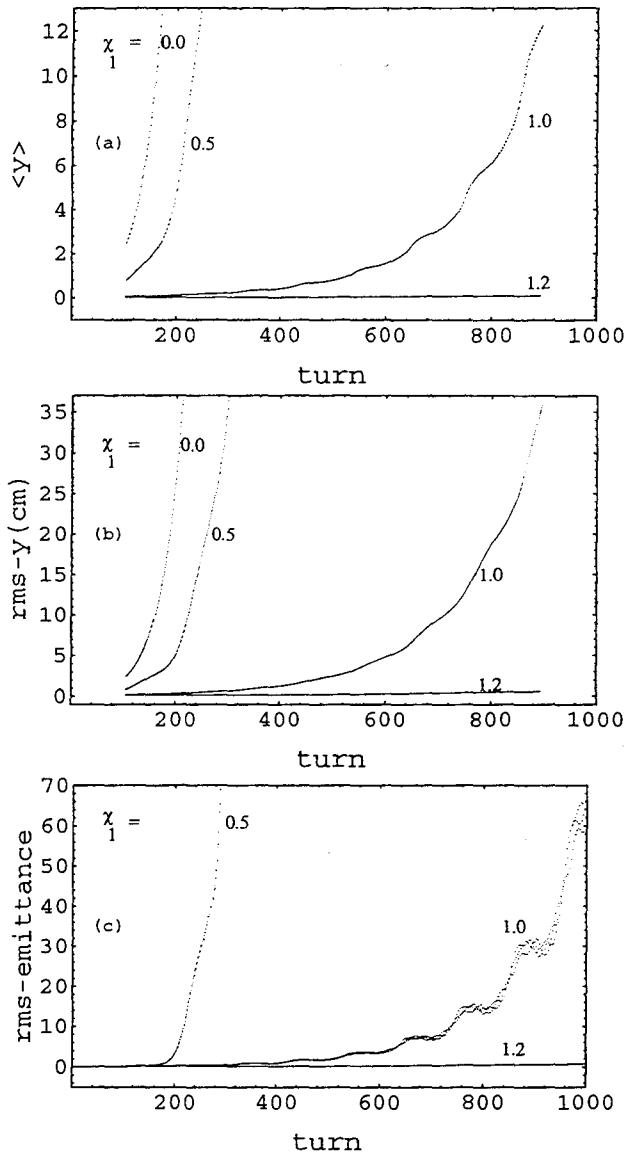

FIG. 16. Multi-particle simulation results showing stabilization of the SHT motions of (a) the centroid, (b) the rms-size and (c) the rms-emittance of a Gaussian beam by χ_1, where the SHT stability limit is $\Upsilon < 1$ (when $\chi_1 = 0$). In these figures, $\chi_0 = 0$, $\Upsilon = 1.65$. See Eqs. (8) and (9) for definitions of χ_0, χ_1, and Υ.